UNIVERSIDADE FEDERAL DO RIO GRANDE DO SUL
ESCOLA DE ENGENHARIA - CURSO DE ENGENHARIA MECÂNICA
TRABALHO DE CONCLUSÃO DE CURSO

EFFECTS OF WATER VAPOR ADDITION ON SOOT FORMATION IN LAMINAR
ETHYLENE COUNTERFLOW FLAMES AND COMPARISON WITH CO_2 ADDITION

por

Matheus Cepik Brune

Monografia apresentada ao Departamento de Engenharia Mecânica da Escola de Engenharia da Universidade Federal do Rio Grande do Sul, como parte dos requisitos para obtenção do diploma de Engenheiro Mecânico.

Porto Alegre, maio de 2021

DADOS INTERNACIONAIS DE CATALOGAÇÃO

Matheus Cepik Brune

EFFECTS OF WATER VAPOR ADDITION ON SOOT FORMATION IN LAMINAR
ETHYLENE COUNTERFLOW FLAMES AND COMPARISON WITH CO_2 ADDITION

<div style="border:1px solid black;">

ESTA MONOGRAFIA FOI JULGADA ADEQUADA COMO PARTE DOS
REQUISITOS PARA A OBTENÇÃO DO TÍTULO DE
ENGENHEIRO MECÂNICO
APROVADA EM SUA FORMA FINAL PELA BANCA EXAMINADORA
DO
CURSO DE ENGENHARIA MECÂNICA

Prof. Mário Roland Sobczyk Sobrinho
Coordenador do Curso de Engenharia Mecânica

</div>

Área de Concentração: Energia e Fenômenos de Transporte

Orientador: Prof. Dr. Fernando Marcelo Pereira
Coorientador: Dr. Eng. Cristian Alex Hoerlle

Comissão de Avaliação:

Profa. Dra. Thamy Cristina Hayashi

Prof. Dr. Andrés Armando Mendiburu Zevallos

Prof. Dr. Paulo Smith Schneider

Porto Alegre, maio de 2021

AGRADECIMENTOS

Agradeço primeiramente aos meus pais, Carla e Osmar, pelo amor, cuidado e estímulo constante à busca de conhecimento.

À minha namorada Bibiana, pelo amor e compreensão que tornaram a minha vida mais leve e feliz durante o percurso acadêmico.

Ao professor Fernando e ao Cristian, pelo aprendizado, paciência e auxílio que tornaram possível a realização deste trabalho.

Ao meu irmão Thiago, pela parceria ao longo dos anos.

À minha família e amigos, por todo apoio durante a caminhada.

A todos os professores que contribuíram para minha formação humana e profissional.

UNIVERSIDADE FEDERAL DO RIO GRANDE DO SUL
ESCOLA DE ENGENHARIA - CURSO DE ENGENHARIA MECÂNICA
TRABALHO DE CONCLUSÃO DE CURSO – 2021

EFFECTS OF WATER VAPOR ADDITION ON SOOT FORMATION IN LAMINAR ETHYLENE COUNTERFLOW FLAMES AND COMPARISON WITH CO$_2$ ADDITION

Cepik Brune, Matheus
matheuscepik@hotmail.com

Abstract. *A numerical investigation of H_2O addition effects on soot formation was performed in laminar counterflow diffusion flames under an oxygen enriched atmosphere. The general flame structure, the chemical effects of H_2O addition and a global comparison between CO_2 and H_2O addition are presented. Water vapor was added either on the fuel or in the oxidizer side, considering the same amount of that species at the flame sheet. Dilution effects were supressed by keeping the C_2H_4 and O_2 concentrations constant for all flames while N_2 is replaced by the added species. The reactive flow was modelled assuming a one-dimensional approximation, soot was modelled by the discrete sectional method and a detailed kinetic mechanism was employed. It was observed that H_2O addition suppresses soot nucleation and surface growth by decreasing H molar fraction through reaction $H_2O + H \rightleftharpoons OH + H_2$, while soot surface oxidation is enhanced mostly by reaction $H_2O + O \rightleftharpoons OH + OH$, which increases OH molar fraction. Addition of H_2O on the fuel side was more effective in inhibiting soot formation than H_2O addition on the oxidizer side. Water vapor and CO_2 additions were compared in different addition levels, which showed that H_2O is a more effective soot suppressor.*

Keywords: *counterflow diffusion flame, water vapor addition, discrete soot sectional method*

NOMENCLATURE

Symbols

x	Axial coordinate	[m]
u	Axial flow velocity	[m s^{-1}]
K	Relative rate of change of mass	[s^{-1}]
p_0	Atmospheric pressure	[N m^{-2}]
MW	Molecular weight	[kg kmol^{-1}]
T	Temperature	[K]
R_u	Universal gas constant	[kJ kg^{-1} K^{-1}]
Y	Mass fraction	-
$\mathcal{D}$	Diffusion coefficient	[m^2 s^{-1}]
c_p	Specific heat at constant pressure	[kJ kg^{-1} K^{-1}]
h	Specific enthalpy	[kJ kg^{-1}]
N_s	Number of species	-
N_{sec}	Number of sections	-
μ	Dynamic viscosity	[kg m^{-1} s^{-1}]
a	Strain rate	[s^{-1}]
v	Volume	[m^3]
X	Molar fraction	-
f_v	Soot volume fraction	-

Greek symbols

ρ	Specific mass	[kg m^{-3}]
$\dot{\omega}$	Rate of production	[kg m^{-3} s^{-1}]
λ	Thermal conductivity coefficient	[W m^{-1} K^{-1}]

Abbreviations and acronyms

DSM	Discrete sectional method
SF	Substitution on the fuel side
SO	Substitution on the oxidizer side
ESO	Equivalent substitution on the oxidizer side
HACA	H-abstraction-C_2H_2-addition
PAH	Polycyclic aromatic hydrocarbon
PSDF	Particle size distribution function

1. INTRODUCTION

The world energetic matrix is highly dependent on combustion processes. According to the International Energy Agency (2019) more than 90% of the global energy consumption comes from combustion. There are many widely known undesirable products of that process, such as nitric oxides (NO_x), carbon monoxid (CO) and soot, which is the focus of this work. Soot consists of solid carbon particles, product of incomplete combustion, with usualy less than 1 μm diameter. These particles harmful effects to human health (NIRANJAN; THAKUR, 2017) and the environment (PRASAD; BELLA, 2011) are well documented. Soot emissions also tend to rise with an increasing urbanization and industrialization, therefore, efforts to suppress soot formation in combustion processes are growing in importance to promote quality of life for the population and ensure environmental sustainability in the long term.

According to Turns (2012), soot formation occurs in a four-step sequence: (1) formation of precursor species, (2) particle inception, (3) surface growth and particle agglomeration and (4) particle oxidation. In the first step, the formation of polycyclic aromatic hydrocarbons (PAHs) is important to the nucleation of the first soot particles. One of the most used and effective approaches to inhibit soot formation is the dilution of fuel or oxidizer with non-fuel species (LIU et al., 2014). This soot suppression occurs through different ways: the dilution effects decrease the reactants concentration; the thermal effects are relative to the change in thermophysical properties of the mixture (mainly its heat capacity); the chemical effects are due to the participation of the diluent species in chemical reactions; the radiation effects occour because of the change in absortion promoted by those species.

Non-premixed flames are widely used in the industry. Their main characteristic is that air and fuel are injected separately and come together through diffusion before burning, which makes the combustion process safer mostly because flashback is eliminated. Diffusion flames in practical applications are mostly turbulent and some examples of their use are found in industrial burners, diesel engines and flares in the oil and gas industry. A simple way to understand a turbulent flame is by considering it a laminar structure, known as flamelet, immersed in a turbulent flow. Turbulence interacts with the flame, stretching or compressing it. Even the smallest turbulent eddies are large compared to the flame thickness, therefore, they do not penetrate the flame, preserving its laminar structure. Counterflow diffusion flames, where turbulence effects are simulated through the imposition of a strain rate, are a good configuration to study the structure of a diffusive flamelet and soot formation using one-dimensional approximations.

Hoerlle and Pereira (2019) studied the influence of CO_2 addition in an oxygen enriched ethylene laminar counterflow diffusion flame on soot formation. The addition of CO_2 on the fuel side (SF) and oxidizer side (ESO) was compared while maintaining the same volume fraction of CO_2 on the flame front. Another studied case (SO) considered the addition of CO_2 on the oxidizer side in the same volumetric fraction of the SF flame, which led to a much greater amount of CO_2 on the flame front. The total dilutions on fuel side and the O_2 mole fraction on the oxidizer side were kept constant through substitution of N_2 by CO_2. The chemical and thermal effects were isolated using a fictitious FCO_2 species and thermal radiation effects were evaluated comparing adiabatic and non-adiabatic solutions. Soot was modelled by the discrete sectional method (DSM), while radiation was computed using the WSGG/DOM approach. The influence of CO_2 addition to soot suppression was similar in the SF and ESO cases, and clearly more pronounced in the SO case, due to a much larger amount of that species in the flame front. Even though chemical and thermophysical effects have equivalent magnitude, it was found that the first are dominant in ESO and SO flames, while the second dominates in the SF flames.

Mahmoud et al. (2019) investigated, numerically and experimentally, the combined influ-

ence of H_2O and CO_2 addition on soot formation in an ethylene laminar counterflow diffusion flame. The effects of each species were evaluated on the fuel and oxidizer sides. The addition on the oxidizer side was performed with the same molar fraction used on the fuel side, thus an equivalent addition on the oxidizer side was not considered. The thermophysical effects were quantified using fictitious FCO_2 and FH_2O species and radiation was computed using the optically thin approximation (OTA). Results showed that H_2O was more efficient than CO_2 in suppressing soot formation for fuel-diluted flames, however the opposite is valid for oxidizer-diluted flames. Simultaneous addition showed a nearly equal effect to the sum of both species addition on both sides, implying that the coupling effect between those species addition is weak.

Kalbhor and Oijen (2020) studied numerically the effects in soot suppression of addition of H_2 on the fuel side and H_2O on the oxidizer side of an ethylene counterflow diffusion flame. The addition of those species decreased soot volume fraction by dilution, thermophysical and chemical effects. Although soot nucleation was increased by the chemical effects, surface growth decreased because both H_2 and H_2O additions inhibit H production, which supresses the H-abstraction step in the H-abstraction-C_2H_2-addition (HACA) mechanism. Dilution and thermophysical effects were more relevant than chemical effects to soot suppression. It was found that the synergistic effects between H_2 and H_2O additions are weak.

This work employs the model proposed by Hoerlle and Pereira (2019) to (1) study the effects of H_2O addition on soot formation in counterflow diffusion flames, presenting a more detailed evaluation of the chemical paths that lead to soot suppression, which has not yet been presented; (2) compare fuel and oxidizer sides addition considering the same content of H_2O in the flame sheet, which has also not been presented; (3) make a global comparison between CO_2 and H_2O additions on fuel and oxidizer sides. A brief discussion about the effects of H_2O addition on the particle size distribution function, absent in the literature, is presented in Appendix B.

2. MATHEMATICAL MODEL

Flat counterflow burners are formed by impingement fuel and oxidizer flows and present a stagnation plane were the axial momentum is zero. In this setup, the flame is usually located at the oxidizer side. In other words, the fuel fuel needs to diffuse through the stagnation plane on the opposite direction of the oxidizer flow until it reaches the stoichiometric mixture, where the flame is formed. Products of combustion and non burned fuel are extracted radially at the stagnation plane. A scheme and a photography of a counterflow diffusion flame are presented in Fig. 1. In this configuration radial gradients are much lower than axial grandients, therefore a one-dimensional set of balance equations in the axial direction represents a good approximation that results in a significant reduction in computational cost and simpler data analysis.

The purpose of this section is to present the mathematical model of counterflow diffusion flames. Soot formation is described by a Sectional Model presented in Sec. 2.3 and the Kaust Mechanism 2.0 (WANG et al., 2013), which is formed by 203 species and 1346 reactions, is employed to model the production/destruction of chemical species up to large aromatics. For the purpose of this work, heat losses by thermal radiation are neglected.

Figure 1 – (a) Burner scheme; (b) Photography of a working counterflow burner. Addapted from Niemann et al. (2014)

(a)   (b)
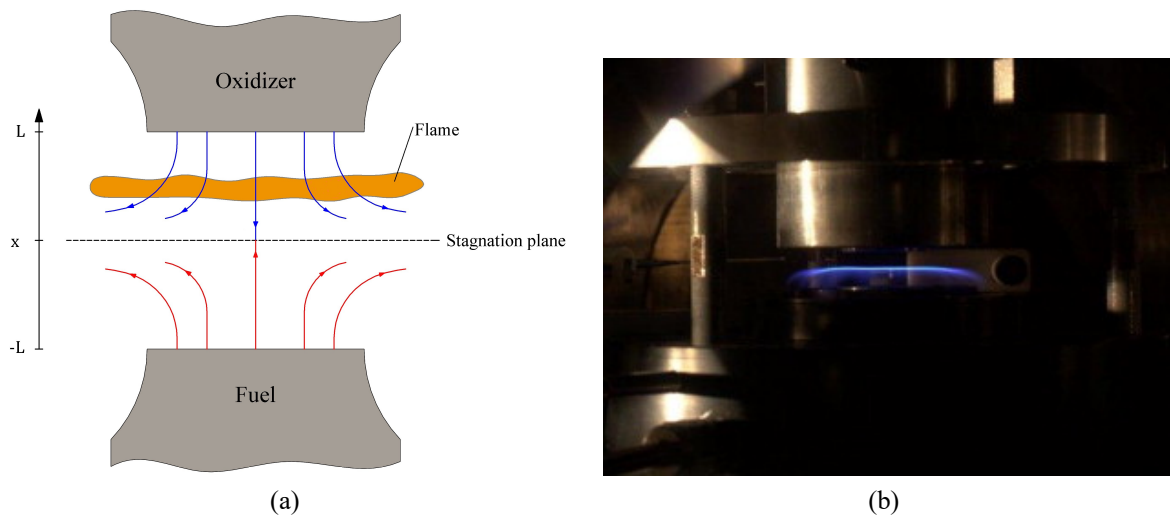
2.1. Conservation equations

A steady-state one-dimensional set of equations is derived from three-dimensional balance equations for reactive flows using the methodology presented by Goey and Boonkkamp (1999).

Conservation of mass is given by

$$\frac{\partial \rho u}{\partial x} = -\rho K, \tag{1}$$

where ρ is the mixture density, x is the axial direction, u is the flow velocity in the x-direction and K is the stretch rate, which will be defined in this section. The right side accounts for the deviations from the one-dimensional condition. For low Mach numbers the flow can be considered incompressible, therefore, the specific mass depends only of temperature, as defined by

$$\rho = \frac{p_0 MW_{mix}}{R_u T}, \tag{2}$$

where p_0 is the atmospheric pressure, MW_{mix} is the molecular weight of the mixture, R_u is the universal gas constant and T is the temperature.

The balance of chemical species i is represented by

$$\frac{\partial \rho u Y_i}{\partial x} = -\frac{\partial}{\partial x}\left(\rho \mathcal{D}_{i,M}\frac{\partial Y_i}{\partial x}\right) + \dot{\omega}_i - \rho K Y_i, \tag{3}$$

where the left side represents the advective transport of species i mass fraction (Y_i). The right side contains the diffusion flux in the axial direction and the net rate of production of species i ($\dot{\omega}_i$), computed based on the Arrhenius formalism, and the deviations from one-dimensional condition, respectively. Diffusion caused by pressure or temperature gradients, known as Soret and Dufour effects, are neglected in this work. The binary diffusion coefficient of species i in the mixture ($\mathcal{D}_{i,M}$) can be defined by

$$\mathcal{D}_{i,M} = \frac{1 - Y_i}{\sum_{i=1,i\neq j}^{N_s}\frac{X_j}{\mathcal{D}_{i,j}}}, \tag{4}$$

where X_j is the molar fraction of species j and the binary diffusion coefficient between species i and j ($\mathcal{D}_{i,j}$) is determined using the Chapman-Enskog theory and the Lennard-Jones parameters (TURNS, 2012). The correction of the diffusion velocity is performed in the abundant species N_2.

The energy conservation equation is given by

$$\frac{\partial \rho u h}{\partial x} = \frac{\partial}{\partial x}\left(\frac{\lambda}{c_p}\frac{\partial h}{\partial x} + \sum_{i=1}^{N_s} -\rho h_i \mathcal{D}_{i,M}\frac{\partial Y_i}{\partial x}\right) - \rho K h, \tag{5}$$

where h is the specific enthalpy of the mixture, which is related to the temperature through $\nabla h = c_p \nabla T$, and N_s is the number of species considered. The left side contains the advective transport of the mixture enthalpy. The right side represents the energy diffusion in the axial direction, including energy transport due to mass diffusion, and the deviations from one-dimensional condition, respectively. The pressure gradients are neglected because the flame is atmospheric, as well as the viscous dissipation because of its small contribution to the heat release.

The stretch rate (K) represents the deviations from the one-dimensional condition and is defined by Oijen and Goey (2000) as the relative rate of change of the mass of an infinitesimal volume of the flame. The transport equation of K is derived from the radial momentum balance equation and defined by

$$\frac{\partial \rho u K}{\partial x} = \frac{\partial}{\partial x}\left(\mu\frac{\partial K}{\partial x}\right) - \rho K^2 + \rho_{ox} a^2, \tag{6}$$

where ρ_{ox} is the density and $a = -\partial u/\partial x$ is the strain rate, both at the oxidizer side. The dynamic viscosity is represented by μ. The one-dimensional domain is defined between $-L$ for the fuel side and $+L$ for the oxidizer side. The stagnation plane is imposed to be located at $x = 0$. Boundary conditions for mass fractions of species, enthalpy of the mixture and stretch rate are presented in Tab. 1.

Table 1 – Boundary conditions for counterflow diffusion flames. Indices f and ox refer to fuel and oxidizer side, respectively.

$$u(x = 0) = 0$$
$$Y_i(x = -L) = Y_{i,f} \qquad Y_i(x = +L) = Y_{i,ox}$$
$$h(x = -L) = h_f \qquad h(x = +L) = h_{ox}$$
$$K(x = -L) = a\sqrt{\rho_{ox}/\rho_f} \quad K(x = +L) = a$$

2.2. Soot formation mechanisms

Soot formation depends on different mechanisms, including formation of precursor species, nucleation, PAH condensation, surface reactions and coagulation. The volumetric rate of soot production is defined as the summation of the source terms associated to those mechanisms. This subsection aims to provide a brief summary of each one of those mechanisms. Extra information about the source terms and surface reactions can be found in Appendix A, but for a more thorough description of the soot formation mechanisms and its mathematical modelling the reader is encouraged to visit Hoerlle (2020).

The PAHs are the main soot precursors. The growth of those aromatics occur through the HACA mechanism, where a -C_2H_2 group is added after an H atom is abstracted from the aro-

matic species. Therefore, the reduction in the concentracion of H and C_2H_2 is capable of supress soot formation.

Soot nucleation, which is a not well understood process yet, marks the transition from gaseous species to the solid particles. In this work it is assumed that soot nucleates from the collision of two pyrene molecules. Pyrene is also the only species assumed to condense on the surface of soot particles, incresing their mass.

Heterogeneous surface reactions play an important role in soot growth and consumption. Surface growth is controled by the HACA mechanism, while oxidation by O_2 and OH radicals accounts for its consumption.

Coagulation involves collision between soot particles. In this work it is assumed that collisions between two particles take place in the coalescence limit, where they are merged togeather into a larger particle, increasing the volume and decreasing its surface area. The particle size distribution is highly dependent on the coagulation process, since it increases particle size and decreases number density.

2.3. The discrete sectional method (DSM)

The purpose of this section is to summarize the governing equations of the Discrete Sectional Method, used to model the soot formation in this work.

Due to limitations of computational power, it is not possible to solve the particle population balance equation continuously for an infinite number of particle sizes. To work around this problem the DSM describes the particle size distribution over a finite number of sections (N_{sec}), solving the transport equation for each one of them. The implementation of the DSM in this work is based on the studies of Hoerlle (2020). The transport equation of soot mass fraction ($Y_{s,i}$) of section i is given by

$$\frac{\partial \rho u Y_{s,i}}{\partial x} = -\frac{\partial \rho u_T Y_{s,i}}{\partial x} + \frac{\partial}{\partial x}\left(\rho \mathscr{D}_{s,i}\frac{\partial Y_{s,i}}{\partial x}\right) + \dot{\omega}_{s,i} + \rho K Y_{s,i}, \tag{7}$$

where $\mathscr{D}_{s,i}$ is a non-physical diffusion coefficient of the soot particles that belong to class i, which is set to be 1% of the average gas diffusivity for numerical reasons. The source term $\dot{\omega}_{s,i}$ is the net rate of soot production/destruction through the processes described in Sec. 2.2. The thermophoretic velocity (u_T) is given by

$$u_T = \frac{3}{4}\left(1 + \frac{\pi \alpha_{acc}}{8}\right)^{-1}\frac{\nu}{T}\frac{\partial T}{\partial x}, \tag{8}$$

where $\alpha_{acc} = 1.0$ is the accomodation factor and ν is the kinematic viscosity.

The particle size distribution is discretized in N_{sec} sections according to

$$v_i = v_{min}\frac{v_{max}}{v_{min}}^{i/N_{sec}}, \tag{9}$$

where the minimum volume, $v_{min} = 3.43 \times 10^{-22}$ cm^3, corresponds to twice the carbon atoms in the soot precursor species, which is pyrene ($C_{16}H_{10}$ or A4). The maximum volume, $v_{max} = 5.30 \times 10^{-12}$ cm^3, is equivalent to a 2163 nm sphere. Taking into account computational cost and accuracy, in this work the number of sections is set to 50.

2.4. Numerical model

The code CHEM1D (SOMERS, 1994) was used to solve the set of one-dimensional steady-state partial differential equations. Since the reactive layer is small compared to the full domain,

a non-uniform grid is used and a refinement is performed in regions with steep gradients. The equations are solved by employing the finite volume method with a fully implicit modified Newton technique. The considered domain of 2.0 cm length is discretized in 400 points with minimum grid size of 1×10^{-2} mm, which showed reasonable agreement with experimental data in Hoerlle and Pereira (2019). The discrete sectional method for soot formation modelling was implemented in CHEM1D by Hoerlle (2020).

3. PROBLEM DEFINITION

The methodology used in this work is based on Hoerlle and Pereira (2019), including boundary conditions, mathematical models, kinetic mechanism and equivalent additions on fuel and oxidizer side. The analysis is expanded to H_2O addition in the present work.

The studied cases are at atmospheric pressure and the strain rate is assumed to be 20 s^{-1}. The fuel of the reference flame consists of 50% C_2H_4 and 50% N_2, while the oxidizer is composed of 28% O_2 and 72% N_2 in molar basis. The temperature of reactants is equal to 400 K. The contents of C_2H_4 in the fuel and O_2 in the oxidizer are kept constant for all flames. Species are added by replacing the N_2 of the fuel or oxidizer mixtures so dilution effects are eliminated and soot formation is only influenced by chemical and thermophysical effects.

Three different types of flames are considered: SF, SO and ESO. Tab. 2 describes those flames.

- SF (substitution on the fuel side) flames are the ones in which the nitrogen of the fuel is replaced by CO_2 or H_2O.

- SO (substitution on the oxidizer side) flames are the ones in which the nitrogen of the oxidizer is replaced by CO_2 or H_2O, with the same mole fractions of the SF flames.

- ESO (equivalent substitution on the oxidizer side) flames are the ones in which the nitrogen of the oxidizer is replaced by CO_2 or H_2O in a way that the amount of those species in a stoichiometric mixture is the same as the obtained in the SF flames.

Table 2 – Species i (CO_2 or H_2O) molar fraction at the boundaries ($X_{i,ox}$ for oxidizer and $X_{i,f}$ for fuel side), for a stoichiometric mixture of reactants (X_i^*) and the stoichiometric mixture fraction Z_{st} for SF, ESO and SO flames. Oxygen molar fraction on the oxidizer side ($X_{O_2} = 0.28$) and ethylene molar fraction on the fuel side ($X_{C_2H_4} = 0.5$) are kept constant for all cases.

Addition level	SF Flames			ESO Flames			SO Flames		
% Vol.	$X_{i,f}$	X_i^*	z_{st}	$X_{i,ox}$	X_i^*	z_{st}	$X_{i,ox}$	X_i^*	z_{st}
10	0.10	0.0157	0.1477	0.0187	0.0157	0.1531	0.10	0.0843	0.1569
20	0.20	0.0315	0.1430	0.0373	0.0315	0.1540	0.20	0.1685	0.1617
30	0.30	0.0472	0.1382	0.0560	0.0472	0.1548	0.30	0.2528	0.1669
40	0.40	0.0629	0.1335	0.0747	0.0629	0.1557	0.40	0.3371	0.1723
50	0.50	0.0787	0.1286	0.0934	0.0787	0.1565	0.50	0.4213	0.1782

To understand how H_2O addition can affect chemically the formation of soot, rate of production analisys (ROP) is used to identify the key reactions affected by the studied species in PAH formation. According to Wang and Frenklach (1997), acetylene (C_2H_2), propargyl radical

(C$_3$H$_3$) and benzene (C$_6$H$_6$ or A1) are crytical species that promote formation of larger PAHs, like pyrene. Monatomic hydrogen is a crucial species to the HACA mechanism.

4. RESULTS

Initially the H$_2$O addition effects on adiabatic counterflow diffusion flames are explored, then a global comparison between CO$_2$ and H$_2$O additions is made.

4.1. Water vapor addition

All the comparisons will be made between SF, ESO, SO and reference flames (zero addition). The H$_2$O addition level presented in the figures of this section is 50%, according to Tab. 2. Since the reactants composition differs between the three in the studied cases, the flame fronts assume distinct positions. Therefore, aiming at an easier comparison, the results are shifted to match the peak position of the reference flame.

4.1.1. General flame structure

The general flame structure of the reference flame is shown in Fig. 2 to provide a better visualization of soot formation in counterflow diffusion flames.

Figure 2 – General flame structure: (a) profiles of temperature and mole fractions of relevant chemical species; (b) profiles of soot volume fraction and A1 and A4 mole fractions; the planes of flow stagnation (x_{st}) and maximum temperature ($x_{T,max}$) are displayed


(a)　　　　　　　　　(b)
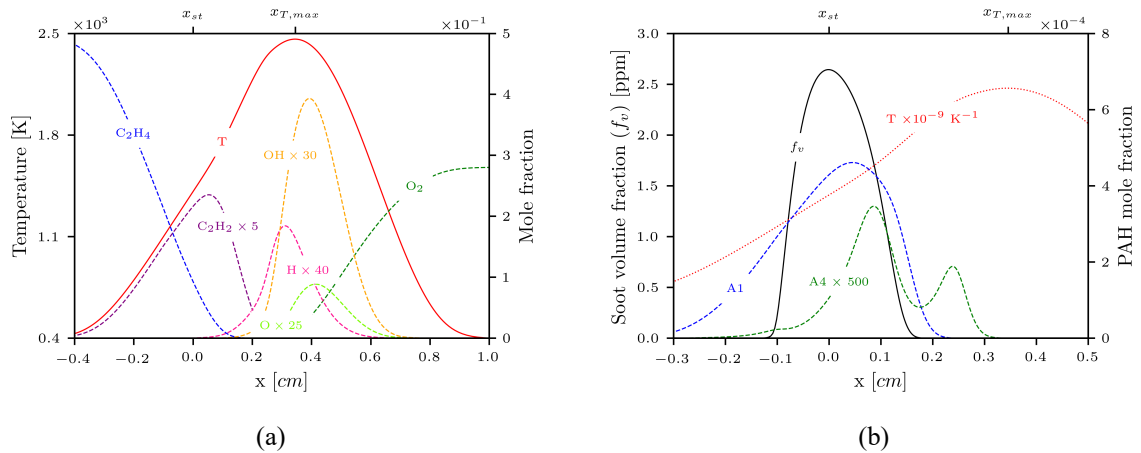
It is possible to see the stagnation plane, imposed at $x_{st} = 0$ cm, and the position of the flame front ($x_{T,max}$). As expected, the concentrations of ethylene and oxygen decrease when these species reach the flame front. The peak of acetylene molar fraction is located on the fuel side of the flame sheet and close to the stagnation plane (Fig. 2(a)). The same occours to the PAHs A1 and A4, although A4 presents a second peak next to the flame sheet (Fig. 2(b)). Monatomic hydrogen, related to soot nucleation and surface growth, and OH, related to surface oxidation, present peaks next to the flame sheet (Fig. 2(a)). Soot nucleation, growth and oxidation by surface reactions, PAH condensation and particle coagulation take place mostly on the fuel side of the flame sheet, as well as the peak of soot volume fraction, located next to the stagnation plane (Fig. 2(b)).

4.1.2. Temperature distribution

The temperature profiles are shown in Fig. 3. The maximum temperature of the reference flame is 2460 K. The difference between maximum temperatures of SF and ESO flames is only 21 K, which is expected because they have a similar H_2O content on the flame sheet. Those temperatures are 2420 K and 2441 K, respectively. Temperature reduction in SO flames is more expressive due to higher H_2O concentrations at the flame front. The maximum temperature of SO flames is 2344 K, which represents a difference of 110 K when compared to the reference flame. Temperature reduction of flames with H_2O addition can be explained by its higher specific heat compared to N_2 and chemical effects.

Figure 3 – Temperature profiles for H_2O addition level of 50%, according to Tab. 2
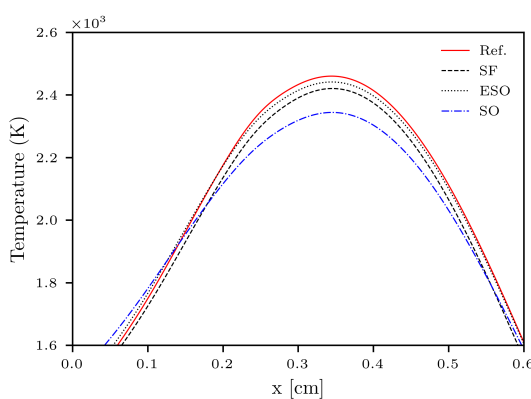
4.1.3. Chemical effects of water vapor addition on soot precursors

Species like C_2H_2, H and H_2 are crucial to soot nucleation and surface growth steps through the HACA mechanism. The H_2 species acts stabilizing PAHs, while H has the opposite effect, creating active sites for C_2H_2 addition. The main responsible for soot oxidation is OH. Molar fractions of those chemical species related to soot formation are presented in Fig. 4.

It is possible to notice that the addition of H_2O reduces H molar fraction by 20% in SF flames, with smaller and larger reductions in ESO and SO flames, respectively. The increase of OH concentration is greater on SO and ESO flames. Molar fractions of C_2H_2 are subjected to small variations, which implies that H is the main species affected by water vapor addition that participates in the HACA mechanism. Concentrations of acetylene slightly decrease in SF flames and increase in SO flames, while its variation in ESO flames is almost imperceptible.

The reduction of H and increase of H_2 and OH concentrations can be attributed to the increased rate of reaction $H_2O + H \rightleftharpoons OH + H_2$ (R1) due to water vapor addition. Molar fractions of OH increase and monatomic oxygen decrease through reaction $H_2O + O \rightleftharpoons OH + OH$ (R2). Both R1 and R2 reaction rates are presented in Fig. 5.

The reason of those small variations in C_2H_2 molar fraction in flames with H_2O addition is that the decrease of monatomic oxygen concentration through R2 decreases acetylene consumption, while the increase of OH concentration through R1 increases it, creating a balance between production and destruction of that species.

The PAHs play an important role in soot formation, since nucleation takes place through collision of two A4 molecules, which can also condense over soot particles. Therefore, it is important to understand the formation of PAHs. Molar fractions of A1, A2, A3 and A4 are presented in Fig. 6. The index corresponds to the number of aromatic rings in the molecule.

Figure 4 – Molar fraction profiles of species involved in soot formation for H_2O addition level of 50%, according to Tab. 2: (a) H; (b) H_2; (c) OH; (d) C_2H_2
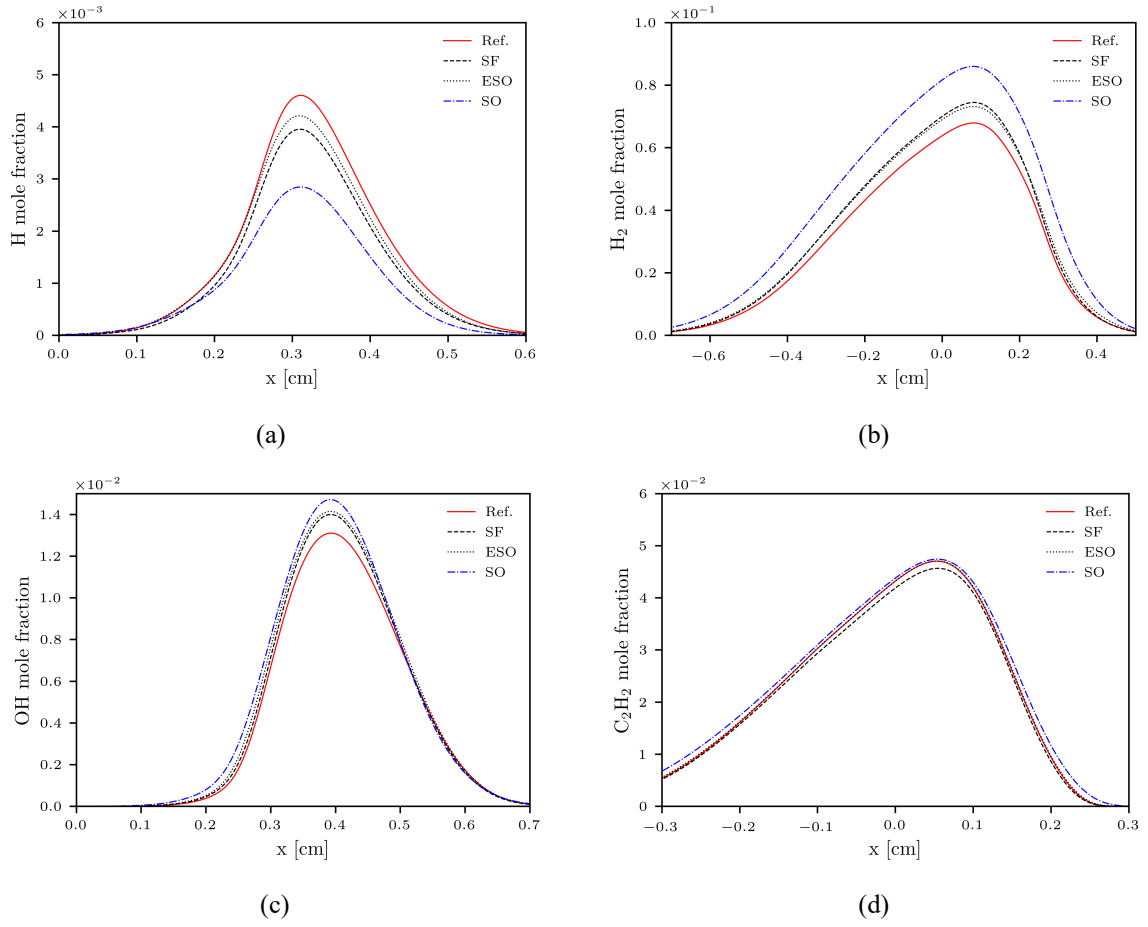

(a)

(b)

(c)

(d)

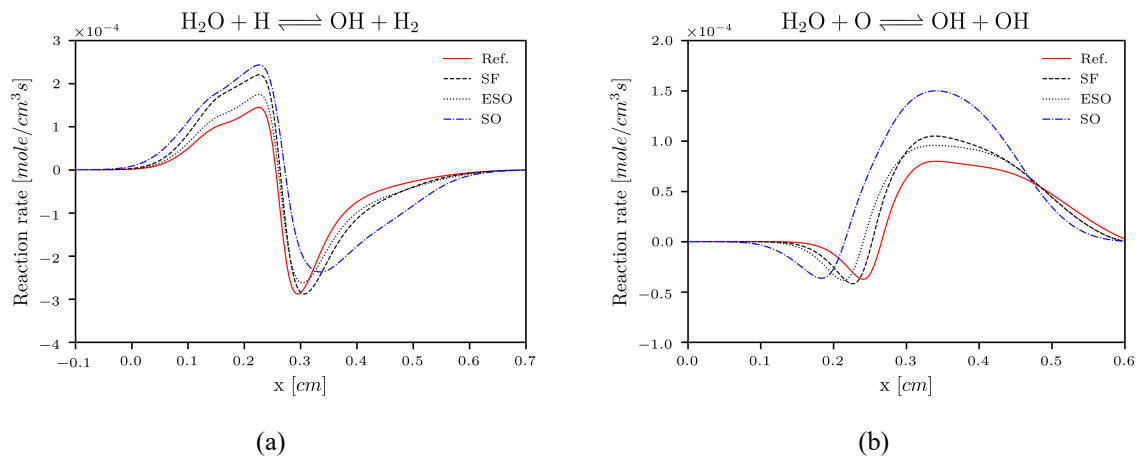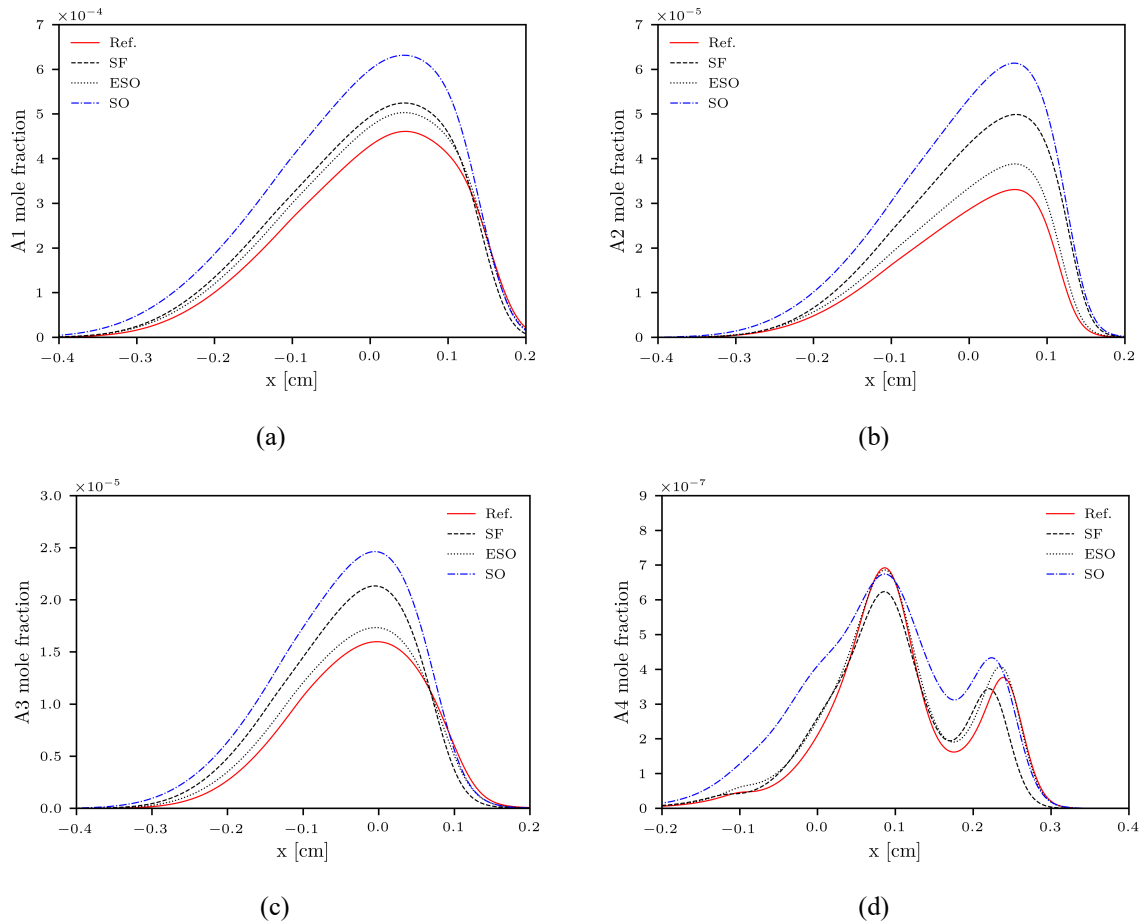Figure 5 – Reaction rates of (a) R1 and (b) R2 for H_2O addition level of 50%, according to Tab. 2

(a)

(b)

Figure 6 – Molar fraction of PAHs for H_2O addition level of 50%, according to Tab. 2: (a) A1; (b) A2; (c) A3; (d) A4

(a)

(b)

(c)

(d)

From Fig. 6, the increse in A1 molar fraction can be explained by elementary reactions. Water vapor addition decreases H molar fraction and increases H_2 concentration (Fig. 4(a) and Fig. 4(b)), which favors the reverse direction of reaction $A1 + H \rightleftharpoons A1^- + H_2$ (R3). Species Ai^- are PAHs with an abstracted H atom, which makes possible the addition of a C_2H_2 molecule to it, resulting in PAH growth. Another reaction affected by H_2O addition is $A1 + H \rightleftharpoons C_4H_5\text{-}2 + C_2H_2$ (R4), because the lower H concentration contribute to decrease the consumption of A1. Reaction rates of R3 and R4 are shown in Fig. 7.

The increase in PAHs A2 and A3 molar fraction in flames with H_2O addition can be explained by reaction $Ai + OH \rightleftharpoons Ai^- + H_2O$ (R5), since the greater amounts of water vapor enhance the rates of its reverse direction. Although a decrease in H concentration in theory tends to produce PAH stabilization, this is not the case when the rates of reaction $Ai + H \rightleftharpoons Ai^- + H_2$ (R6) are analyzed for those two species. This counterintuitive result will be better explained along with the effects of water vapor addition on A4 molar fraction.

To better understand the effects of water vapor addition on soot nucleation it is important to analyze its influence in A4 formation. From Fig. 6(d) it is possible to notice that A4 concentrations decrease in SF flames and increase in SO flames, while remaining practically the same in ESO flames. According to Kalbhor and Oijen (2020) reactions $A3C_2H_2 \rightleftharpoons A_4 + H$ (R7) and $A3^- + C_2H_2 \rightarrow A4 + H$ (R8) are primarily responsible for the first peak of the A4 molar fraction profile. The rates of reactions R7 and R8 are presented in Fig. 8.

Figure 7 – Main reactions affected by water vapor addition involved in the formation of A1 for H_2O addition level of 50%, according to Tab. 2: (a) R3; (b) R4
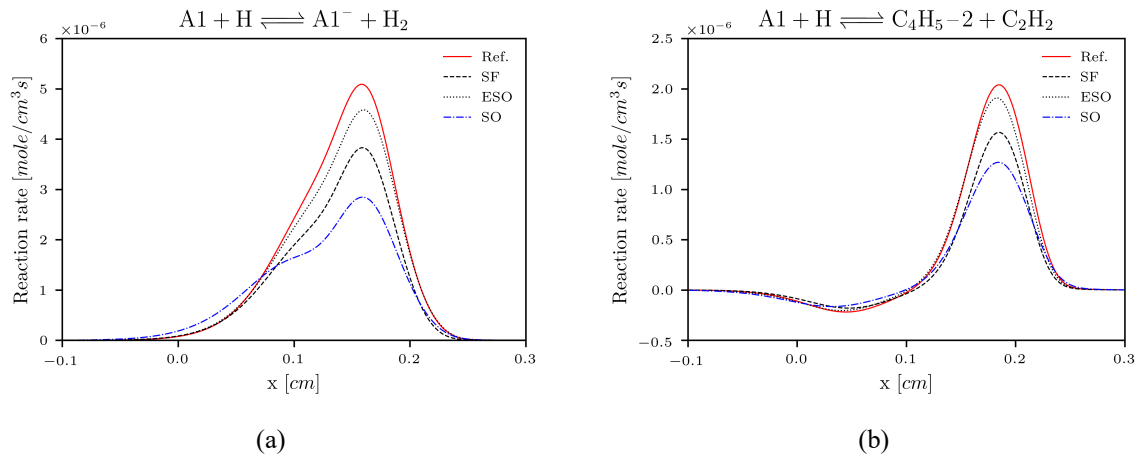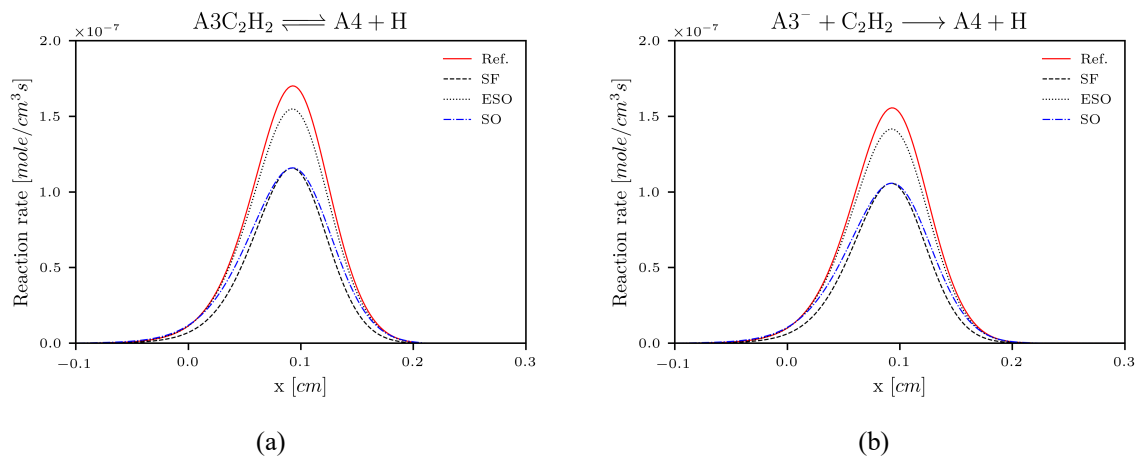

(a)

(b)

Figure 8 – Rates of reactions responsible for the first peak of A4 molar fraction for H_2O addition level of 50%, according to Tab. 2: (a) R7; (b) R8


(a)

(b)

Although H molar fraction decreases, there is a significant and similar reducion in the rates of R7 and R8 for SF and SO flames, limiting A4 production. The reason for that is the decrease in $A3^-$ concentration, which is produced by $A2R5^- + C_2H_2 \rightleftharpoons A3^-$ (R9) and is the main precursor species of $A3C_2H_2$. The concentration of $A2R5^-$, which depends of reaction $A2R5 + H \rightleftharpoons A2R5^- + H_2$ (R10), is decreased due to the lower H molar fractions presented in flames with H_2O addition. The lower rates of R9 in SF compared to SO flames are due to a marginal reduction on C_2H_2 concentration in SF flames, as can be seen from Fig. 4(d). Species A2R5, acenaphthylene, is an intermediate tricyclic PAH between A2 and A3. Reaction rates of R9 and R10 are shown in Fig. 9.

An important aspect of the influence of H_2O addition in counterflow diffusion flames in the production of certain species is that, although some reactions are affected in the opposite way to the expected, e.g., the reduction of R7 and R8 reaction rates given the lower H molar fractions, other reaction rates are affected by the H concentration reduction exactly as expected, e.g., the decrease of R10 reaction rates. Thus, great non-linearities are generated by water vapor addition, given the influence of R10 on R7 and R8, which makes the analysis of H_2O effects on PAHs

formation sometimes complicated, requiring a more detailed investigation of the ROPs.

Figure 9 – Rates of reactions related to A4 precursor $A3^-$ production for H_2O addition level of 50%, according to Tab. 2: (a) R9; (b) R10

(a)

(b)
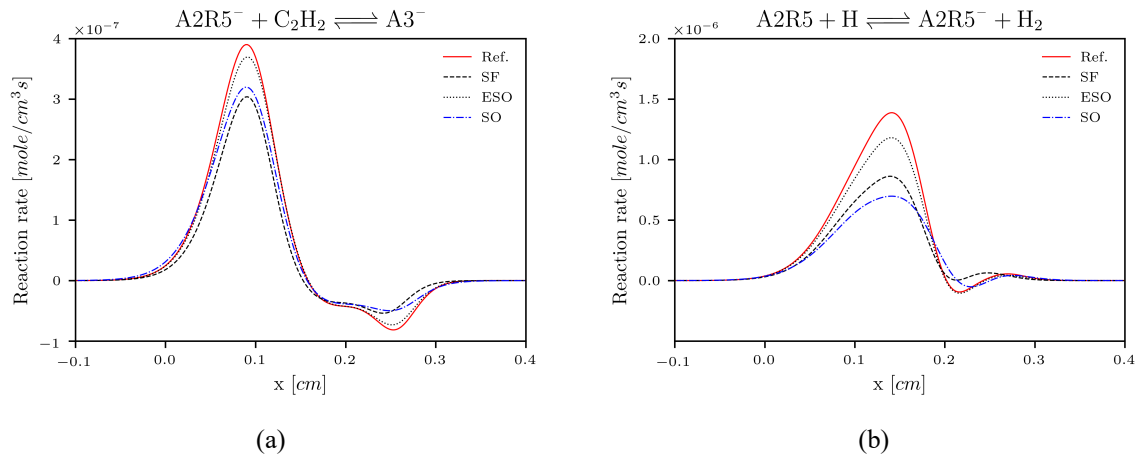
According to Hoerlle and Pereira (2019), the second peak of A4 molar fraction, Fig. 6(d) at $x \approx 0.25$ cm, is caused by reactions $A4 + H \rightleftharpoons A4^- + H_2$ (R11) and $A4 + OH \rightleftharpoons A4^- + H_2O$ (R12). Reaction R11 is practicly canceled by reaction $A4^- + H \rightleftharpoons A4$ (R13), since they occour in reverse directions of production/destruction of A4 and present similar rates. Therefore, R12 controls the balance between A4 and $A4^-$ and its reaction rate profiles are presented in Fig. 10.

Figure 10 – Reaction rate profiles of R12, that controls the balance between A4 and $A4^-$, for H_2O addition level of 50%, according to Tab. 2
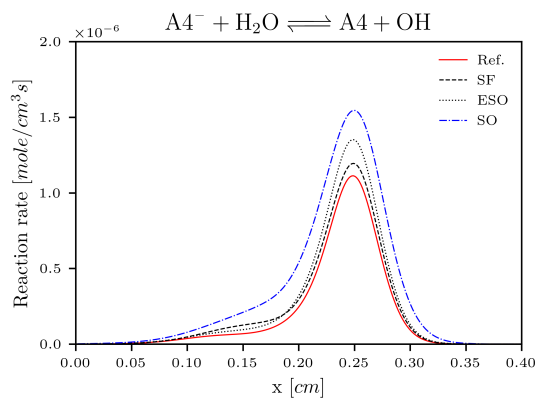

The rates of reaction R12 are consistent with the profiles of the second peak of A4 molar fraction, since ROPs of A4 are higher in ESO and SO flames. The increased reaction rates in those flames is due to higher concentrations of H_2O in the region of the second peak.

4.1.4. Chemical effects of water vapor addition on soot formation and consumption

With the previous discussions, we are better prepared to relate the souce terms of soot nucleation, surface growth and surface oxidation to the chemical effects of water vapor addition, therefore, those quantities are presented in Fig. 11.

Figure 11 – Soot source terms profiles and volume fraction for H_2O addition level of 50%, according to Tab. 2: (a) soot nucleation; (b) soot surface growth; (c) soot oxidation; (d) soot volume fraction (f_v)

(a)

(b)

(c)

(d)
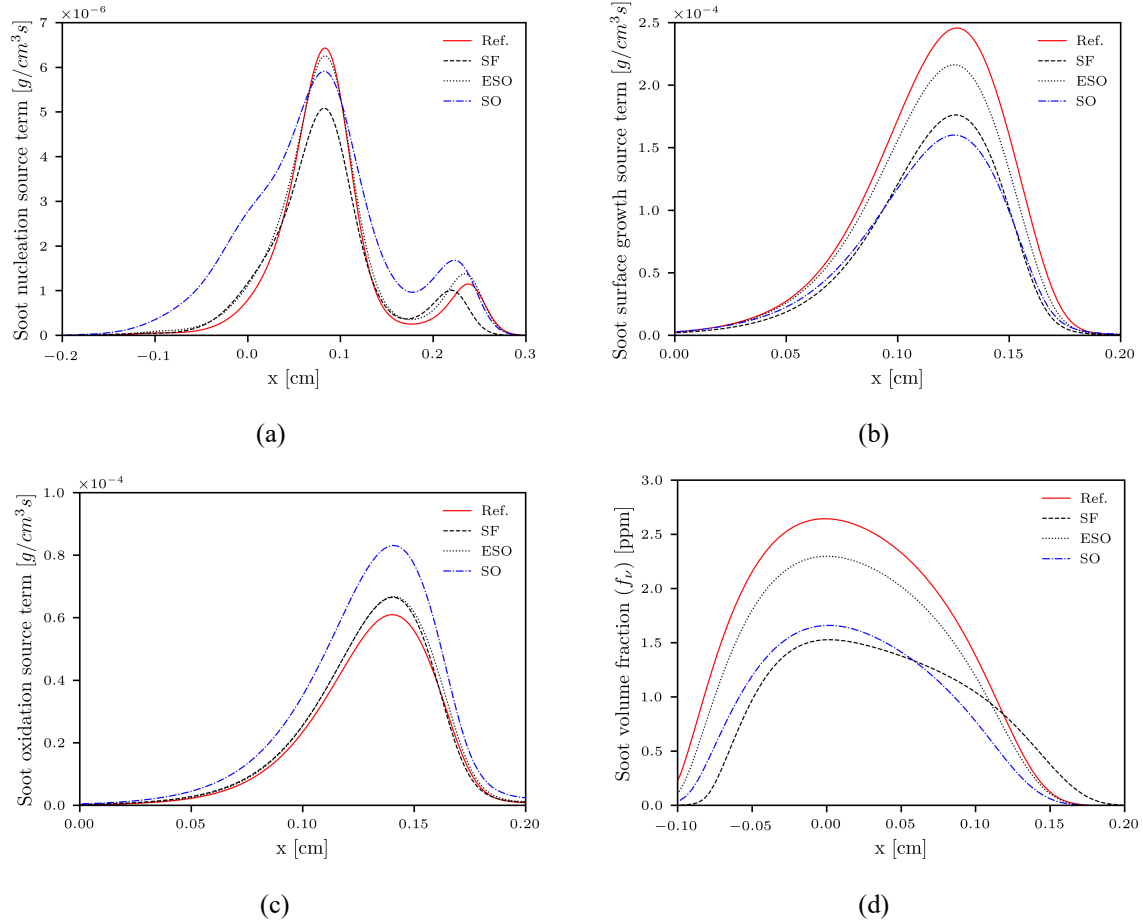
Nucleation source term profiles, Fig, 11(a), are very similar to the A4 molar fraction profile, Fig. 6(d). That resemblance is extremily justified, because, as mentioned in Sec. 2.2, nucleation takes place through collision of two A4 molecules. Evaluating the area beneath the curves it is possible to notice that SO flames nucleate the most, followed respectively by ESO, reference and SF flames. Thus, fuel side addition is much more capable of suppressing soot nucleation.

Surface growth is highly dependent on H and H_2 molar fraction, because the addition of C_2H_2 depends on the creation of active (dehydrogenated) sites through $C_{soot} + H \rightleftharpoons C^*_{soot} + H_2$ (R14). Therefore, the results presented in Fig. 11(b) are consistent with the lower concentrations of H and higher concentrations of H_2, presented in Fig. 4(a) and Fig. 4(b), respectively. Surface growth presents a small reduction in ESO flames and a larger decrease in SF and SO flames. Therefore, the addition of water vapor on the fuel side is more efficient in minimizing soot surface growth rate. This increased efficiency is evident by the larger suppression of H and formation of H_2 in SO flames, which does not correspond to an equivalent reduction in surface growth when compared to the SF flames. Addition of H_2O on the fuel side creates a larger concentration of water in the fuel rich side of the flame, where soot formation reactions are important.

Surface oxidation depends mostly on OH molar fraction and is presented in Fig. 11(c). Water vapor addition increases the oxidation rates similarly in SF and ESO flames, while these rates present a larger increment in SO flames because of their higher OH molar fractions (Fig. 4(c)).

The combination of those source terms determines the volumetric fraction of soot, presented in Fig. 11(d). According to Fig. 11(a) and Fig. 11(b), soot nucleates and grows on the fuel side relative to the flame sheet, and is convected to the region around the stagnation plane. Soot volume fraction of SO flames is higher compared to SF flames, even though SO flames present a much higher quantity of water vapor. That shows fuel side addition of H_2O is much more efficient in inhibiting soot formation in counterflow diffusion flames.

A discussion about the influence of water vapor addition in soot particle size distribution functions is presented in Appendix B.

4.2. Comparison between H_2O and CO_2 addition

In this section a global comparison between the addition of H_2O and CO_2 on counterflow diffusion flames is made considering the addition levels presented in Tab. 2. The analyzed quantities are peak temperature and the integration of soot volume fraction ($\int f_v dx$).

Figure 12 – Relative change of (a) peak temperature and (b) integrated soot volume fraction in respect to the reference flame for CO_2 and H_2O in different addition levels, according to Tab. 2

(a)   (b)
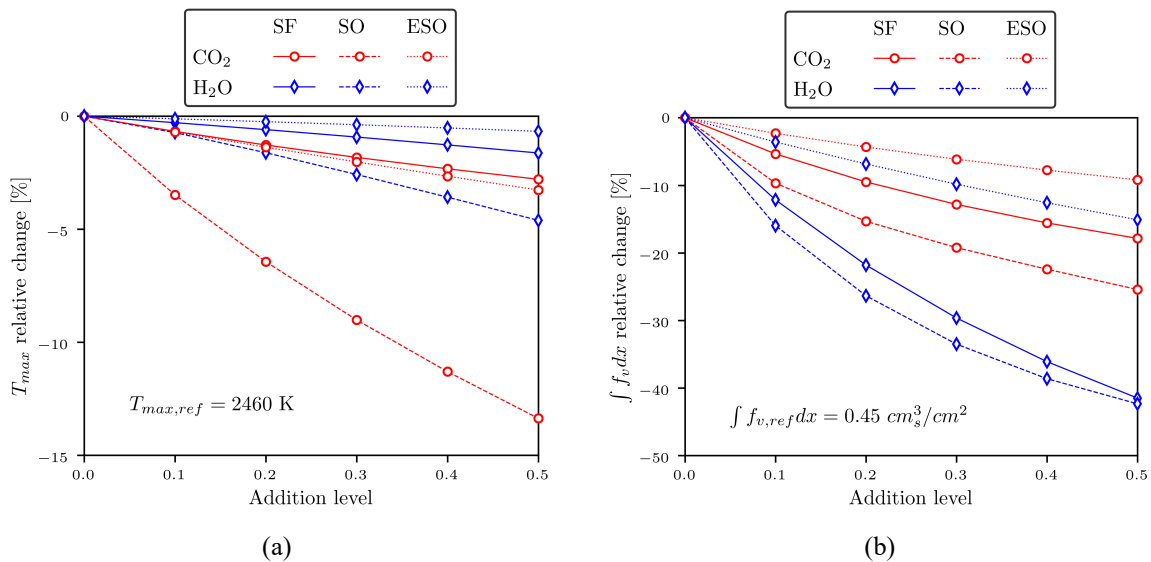
According to Fig. 12(a), flames with H_2O addition present higher peak temperatures. The values of relative reduction considering the 50% addition level of water vapor for ESO, SF and SO flames are 0.8%, 2% and 5%, respectively. Considering the same addition level of CO_2 the relative reductions are 3%, 3% and 13% respectively for ESO, SF and SO flames. Those higher temperatures of flames with H_2O addition are related to chemical effects and mainly to the higher specific heat of CO_2 compared to water vapor.

From Fig. 12(b) it is possible to conclude that soot formation decreases when the addition levels increase and that H_2O is more efficient than CO_2 in suppressing soot formation, which agrees with Mahmoud et al. (2019) for fuel side, but not for oxidizer side addition. The values of relative reduction of the integration of soot volume fraction considering the 50% addition level of water vapor for ESO, SF and SO flames are 15%, 41% and 42%, respectively. Considering the same addition level of CO_2 the relative reductions are 9%, 18% and 25% respectively for ESO, SF and SO flames. Therefore, H_2O is a better soot suppressor than CO_2 for the three types os flames.

The main qualitative difference between the addition of those two species is that, for CO_2 addition, soot volume fraction always follows the well defined sequence ESO > SF > SO, while

for H_2O addition, the difference between SF and SO flames soot suppression is lower. That difference presents an increse at intermediate addition levels and a reduction at high addition levels. Those lower differences are a surprising result, given that the quantity of water vapor in SO flames is much higher than in SF flames. Thus, while H_2O addition on the fuel side (SF) is much more efficient in inhibiting soot formation than oxidizer side addition (ESO), CO_2 addition on the fuel side is just slightly more efficient.

Appendix C presents a brief discussion about the coupling effects of fuel side combined addition of H_2O and CO_2.

5. CONCLUSION

The effects of water vapor addition on soot formation in ethylene counterflow diffusion flames were numerically evaluated in this work. The reactive flow was modelled using a one-dimensional approximation and soot was modelled by the discrete sectional method. The methodology used by Hoerlle and Pereira (2019) to study the effects of CO_2 on soot formation in those flames was used to evaluate the H_2O addition. Water vapor was added on the fuel side, on the oxidizer side with the same molar fraction and on the oxidizer side with equivalent substitution (SF, SO and ESO flames). The results of those cases were compared to understand the differences between fuel and oxidizer side additions.

Initially counterflow diffusion flames general structure was analyzed, which showed that the peak of soot volume fraction takes place at the stagnation plane, on the fuel side relative to the flame sheet. It was found that water vapor addition decreases the maximum temperatures of counterflow diffusion flames. The greatest reduction occured on SO flames, followed by SF and ESO flames. Those lower temperatures are explained by chemical effects and the higher specific heat of H_2O compared to N_2.

Water vapor addition results in lower soot volume fractions by decreasing soot nucleation rates on SF flames due to a reduction in pyrene molar fraction. This reduction is caused mostly by reaction $H_2O + H \rightleftharpoons OH + H_2$ that lowers H concentration, affecting the HACA mechanism. Soot surface growth is decreased because of the same reaction, since H is responsible for creating active sites for C_2H_2 addition on soot particles. The rates of surface oxidation increased due to higher concentrations of OH caused by the augmented rate of reaction $H_2O + O \rightleftharpoons OH + OH$.

Fuel side addition of H_2O was proven to be more efficient in suppressing soot formation, while oxidizer side addition promoted only a marginal suppresion in ESO flames. The SO flames presented a similar, however lower, reduction in soot volume fraction compared to SF flames due to a much higher amount of H_2O in the SO case. That reduction is caused by a drecrease in surface growth and an increase in oxidation, despite the increment in soot nucleation.

Finally, a global comparison between H_2O and CO_2 additions was conducted. Water vapor addition results in higher flame temperatures and lower soot volume fractions compared to CO_2 addition. Both species showed a better capacity of reducing soot volume fraction when added on the fuel side (SF) rather than in the oxidizer side (ESO). Addition of CO_2 presented lower differences between fuel and oxidizer sides compared to H_2O addition, in which SF and SO flames showed a similar soot suppression effect, much higher than in ESO flames.

For future works the author suggests using fictitious species addition, a method that works by introducing species that do not participate in chemical reactions but produce the expected changes in the thermophysical properties of the mixture, making possible to quantify the chemical and thermophysical effects on soot suppression separately. Heat exchanged by thermal radiation is extremely important in diffusion flames and its effects on soot formation are significant, therefore, it is important to take it into consideration to evaluate the effects of H_2O or CO_2 addition in counterflow diffusion flames.

BIBLIOGRAPHIC REFERENCES

GOEY, L. de; BOONKKAMP, J. ten T. A flamelet description of premixed laminar flames and the relation with flame stretch. **Combustion and Flame**, Elsevier BV, v. 119, n. 3, p. 253–271, nov. 1999. Available from: <https://doi.org/10.1016/s0010-2180(99)00052-8>.

HOERLLE, C. A. **Modeling of soot formation based on the discrete sectional method: CO_2 effects and coupling with the FGM technique**. Thesis (Phd in Mechanical Engineering) — Federal University of Rio Grande do Sul, 2020.

HOERLLE, C. A.; PEREIRA, F. M. Effects of CO_2 addition on soot formation of ethylene non-premixed flames under oxygen enriched atmospheres. **Combustion and Flame**, Elsevier BV, v. 203, p. 407–423, maio 2019. Available from: <https://doi.org/10.1016/j.combustflame.2019.02.016>.

International Energy Agency. **Key world energy statistics**. 2019.

KALBHOR, A.; OIJEN, J. van. Effects of hydrogen enrichment and water vapour dilution on soot formation in laminar ethylene counterflow flames. **International Journal of Hydrogen Energy**, Elsevier BV, v. 45, n. 43, p. 23653–23673, set. 2020. Available from: <https://doi.org/10.1016/j.ijhydene.2020.06.183>.

LIU, F.; CONSALVI, J.-L.; FUENTES, A. Effects of water vapor addition to the air stream on soot formation and flame properties in a laminar coflow ethylene/air diffusion flame. **Combustion and Flame**, Elsevier BV, v. 161, n. 7, p. 1724–1734, jul. 2014. Available from: <https://doi.org/10.1016/j.combustflame.2013.12.017>.

MAHMOUD, N. M. et al. Coupled effects of carbon dioxide and water vapor addition on soot formation in ethylene diffusion flames. **Energy & Fuels**, American Chemical Society (ACS), v. 33, n. 6, p. 5582–5596, maio 2019. Available from: <https://doi.org/10.1021/acs.energyfuels.9b00192>.

NIEMANN, U.; SESHADRI, K.; WILLIAMS, F. A. Methane, ethane, and ethylene laminar counterflow diffusion flames at elevated pressures: Experimental and computational investigations up to 2.0mpa. **Combustion and Flame**, Elsevier BV, v. 161, n. 1, p. 138–146, jan. 2014. Available from: <https://doi.org/10.1016/j.combustflame.2013.07.019>.

NIRANJAN, R.; THAKUR, A. K. The toxicological mechanisms of environmental soot (black carbon) and carbon black: Focus on oxidative stress and inflammatory pathways. **Frontiers in Immunology**, Frontiers Media SA, v. 8, jun. 2017. Available from: <https://doi.org/10.3389/fimmu.2017.00763>.

OIJEN, J. V.; GOEY, L. D. Modelling of premixed laminar flames using flamelet-generated manifolds. **Combustion Science and Technology**, Informa UK Limited, v. 161, n. 1, p. 113–137, dez. 2000. Available from: <https://doi.org/10.1080/00102200008935814>.

PRASAD, R.; BELLA, V. R. A review on diesel soot emission, its effect and control. **Bulletin of chemical reaction engineering and catalysis**, Bulletin of Chemical Reaction Engineering and Catalysis, v. 5, n. 2, jan. 2011. Available from: <https://doi.org/10.9767/bcrec.5.2.794.69-86>.

SOMERS, L. **The simulation of flat flames with detailed and reduced chemical models**. Thesis (Phd in Mechanical Engineering) — Technische Universiteit Eindhoven, 1994.

TURNS, S. R. **An introduction to combustion: Concepts and applications**. 3. ed. New York, NY: McGraw-Hill Co., 2012.

WANG, H.; FRENKLACH, M. A detailed kinetic modeling study of aromatics formation in laminar premixed acetylene and ethylene flames. **Combustion and Flame**, Elsevier BV, v. 110, n. 1-2, p. 173–221, jul. 1997. Available from: <https://doi.org/10.1016/s0010-2180(97)00068-0>.

WANG, Y.; RAJ, A.; CHUNG, S. H. A PAH growth mechanism and synergistic effect on PAH formation in counterflow diffusion flames. **Combustion and Flame**, Elsevier BV, v. 160, n. 9, p. 1667–1676, set. 2013. Available from: <https://doi.org/10.1016/j.combustflame.2013.03.013>.

APPENDIX A

This appendix aims to provide a resumed overview of the mathematical modelling of soot source terms, which are present in the transport equation of soot mass fraction (Equation 7).

Nucleation takes place only in the first section through the collision of two A4 molecules and its source term is defined in

$$\dot{Q}_{1,nuc} = 2v_{A4}\beta_{A4,A4}N_{A4}^2, \tag{A.1}$$

where v_{A4} is the volume of an A4 molecule, $\beta_{A4,A4}$ is the collision frequency between A4 molecules and N_{A4} is the A4 number density.

Condensation of A4 molecules on the surface of soot particles is modelled by

$$\Delta\dot{Q}_{i,cond} = v_{A4}N_{A4}\int_{v_{i,min}}^{v_{i,max}} \beta_{A4,i}n_i(v)dv, \tag{A.2}$$

where $\beta_{A4,i}$ is the collision frequency between A4 molecules and soot particles of section i and $n_i(v)$ is the nuber density distribution of soot.

The main reactions between soot surface and gas phase species are presented in Tab. A.1.

Table A.1 – Soot-gas surface reactions. $C_{soot,n}$ represents the saturated sited and $C^*_{soot,n}$ represents the active sites available for C_2H_2 addition. Index n represents the number of carbon atoms in the soot particle and γ_{OH} is the collision probability for SR6. Addapted from Hoerlle and Pereira (2019).

No.	Reaction	$k = AT^b \exp(-E_a/RT)$		
		A $\mathrm{cm^3mol^{-1}s^{-1}}$	b	E_a kcal/kmol
SR1$_f$	$C_{soot,n} + H \rightleftharpoons C^*_{soot,n} + H_2$	4.2×10^{13}	0.0	13.0
SR1$_r$		3.9×10^{12}	0.0	11.0
SR2$_f$	$C_{soot,n} + OH \rightleftharpoons C^*_{soot,n} + H_2O$	1.0×10^{10}	0.734	1.43
SR2$_r$		3.68×10^8	1.139	17.1
SR3	$C^*_{soot,n} + H \rightarrow C_{soot,n}$	2.0×10^{13}	0.0	0.0
SR4	$C^*_{soot,n} + C_2H_2 \rightarrow C^*_{soot,n+2} + H$	8.0×10^{10}	1.560	3.8
SR5	$C^*_{soot,n} + O_2 \rightarrow C^*_{soot,n-2} + 2\,CO$	2.2×10^{12}	0.0	7.5
SR6	$C^*_{soot,n} + OH \rightarrow C^*_{soot,n-1} + CO$		$\gamma_{OH} = 0.13$	

From the reaction constants or collision probability of SR4, SR5 and SR6 it is possible to define the source terms of surface growth, based on the HACA mechanism, and oxidation through OH and O_2. A more detailed mathematical modelling of soot source terms can be found in Hoerlle (2020), including coagulation and intersectional dynamics.

APPENDIX B

Particle size distribution functions are presented in Fig. B.1 at locations equivalent to fractions of 10%, 50%, 75% and 100% of the maximum soot volume fraction ($f_{v,max}$) on the oxidizer side. According to Hoerlle and Pereira (2019) the PSDF changes from unimodal to bimodal decay between 10% and 50% of $f_{v,max}$ because of a competition between nucleation and coagulation. The region between the two modes is known as the trough. As nucleation and, therefore, coagulation source terms grow the trough is deslocated to smaller particle diameters. At 75% of $f_{v,max}$ the PSDF of the SF flames separates from the others because of its lower nucleation and surface growth source term. At 100% of $f_{v,max}$ the distinction between the troughs becomes more apparent, caused by the difference between nucleation source terms. Since SO flames nucleates the most they present a higher quantity of small particles, followed by ESO, reference and SF flames respectively. It is possible to notice in the four positions that H_2O addition limitates the number of higher diameter particles.

Figure B.1 – Particle size distribution functions for H_2O addition level of 50%, according to Tab. 2 at: (a) 10% of $f_{v,max}$; (b) 50% of $f_{v,max}$; (a) 75% of $f_{v,max}$ and (a) 100% of $f_{v,max}$

(a)

(b)

(c)

(d)
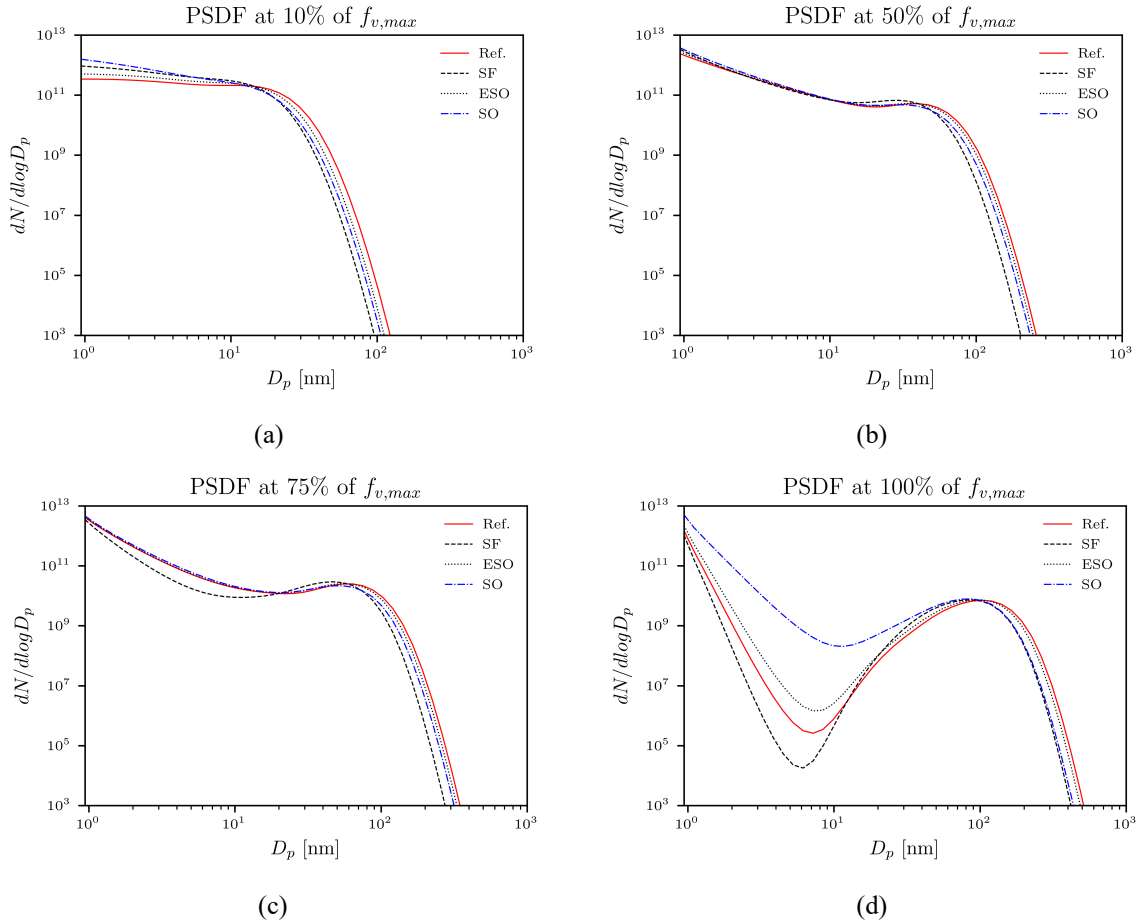
APPENDIX C

This appendix presents comparisons to identify a possible coupling effect when additions of water vapor and carbon dioxide are combined. A comparison of soot volume fraction profiles for SF flames with different compositions is presented in Fig. C.2. Addition levels of 50% were considered and the combined addition consists in 25% of H_2O and 25% of CO_2.

Figure C.2 – Comparison between the combined and individual fuel side additions of H_2O and CO_2 for an addition level of 50%, according to Tab. 2
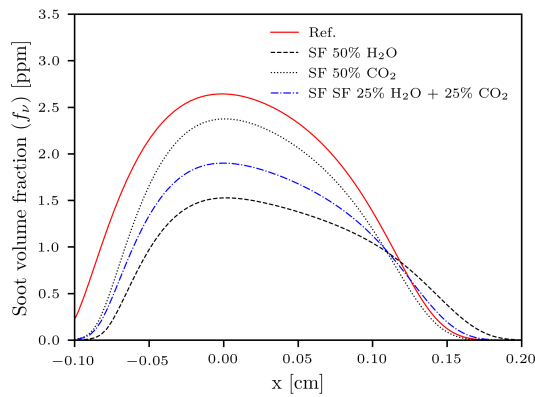
The soot volume fraction profile for the combined addition is located in an intermediate position relative to the profiles of H_2O and CO_2 addition. A quantification of the relative differences is made based on the integration of soot volume fraction, as shown in Tab. C.2.

Table C.2 – Integration of soot volume fraction and its relative difference based on reference flame

Comparison cases	$\int f_v dx \times 10^6$	Relative difference
Reference	0.45	-
50% H_2O	0.26	-41.5%
50% CO_2	0.37	-17.9%
25% H_2O + 25% CO_2	0.31	-30.6%

Since the relative difference of the integration of soot volume fraction for combined addition is very close to the average between individual H_2O and CO_2 addition, it possible to conclude that the coupling effects between water vapor and carbon dioxide addition in soot suppression are weak, the same conclusion obtained by Mahmoud et al. (2019).